

High-pressure synergetic measurement station (HP-SymS)

Xiaohui Yu(于晓辉), Fangfei Li(李芳菲), Yonghao Han(韩永昊), Fang Hong(洪芳), Changqing Jin(靳常青), Zhi He(何志), Qiang Zhou(周强)

Citation: Chin. Phys. B . 2018, 27(7): 070701. **doi:** 10.1088/1674-1056/27/7/070701

Journal homepage: http://cpb.iphy.ac.cn; http://iopscience.iop.org/cpb

What follows is a list of articles you may be interested in

Sub-millikelvin station at Synergetic Extreme Condition User Facility

Zhi Gang Cheng(程智刚), Jie Fan(樊洁), Xiunian Jing(景秀年), Li Lu(吕力)

Chin. Phys. B . 2018, 27(7): 070702. **doi:** 10.1088/1674-1056/27/7/070702

Microwave coherent manipulation of cold atoms in optically induced fictitious magnetic traps on an atom chip

Feng Zhou(周锋), Xiao Li(李潇), Min Ke(柯敏), Jin Wang(王谨), Ming-Sheng Zhan(詹明生)

Chin. Phys. B . 2017, 26(9): 090701. **doi:** 10.1088/1674-1056/26/9/090701

Raman sideband cooling of rubidium atoms in optical lattice

Chun-Hua Wei(魏春华), Shu-Hua Yan(颜树华)

Chin. Phys. B . 2017, 26(8): 080701. **doi:** 10.1088/1674-1056/26/8/080701

Ferromagnetic materials under high pressure in a diamond-anvil cell：A magnetic study

Wang Xin, Hu Tian-Li, Han Bing, Jin Hui-Chao, Li Yan, Zhou Qiang, Zhang Tao

Chin. Phys. B . 2014, 23(7): 070701. **doi:** 10.1088/1674-1056/23/7/070701

TOPICAL REVIEW — Synergetic Extreme Condition User Facility: Breakthroughs and opportunities for the research of physical science

High-pressure synergetic measurement station (HP-SymS)*

Xiaohui Yu(于晓辉)[1,†,‡], Fangfei Li(李芳菲)[2,†], Yonghao Han(韩永昊)[2,†], Fang Hong(洪芳)[1], Changqing Jin(靳常青)[1], Zhi He(何志)[2], and Qiang Zhou(周强)[2,§]

[1] *Beijing National Laboratory for Condensed Matter Physics, Institute of Physics, Chinese Academy of Sciences, Beijing* 100190, *China*
[2] *State Key Laboratory of Superhard Materials, College of Physics, Jilin University, Changchun* 130012, *China*

(Received 10 April 2018; revised manuscript received 13 May 2018; published online 1 June 2018)

In the High-Pressure Synergetic Measurements Station (HP-SymS) of the Synergic Extreme Condition User Facility (SECUF), we will develop ultrahigh-pressure devices based on diamond-anvil cell (DAC) techniques, with a target pressure up to 300 GPa. With the use of cryostat and magnet, we will reach 300 GPa–4.2 K–9 T and conduct simultaneous measurements of the electrical-transport property and Raman/Brillouin spectrascopy. With resistance heating and laser heating, we will reach temperatures of at least 1000 and 3000 K, respectively, coupled with Raman/Brillouin spectroscopy measurements. Some designs of supporting devices, such as a femtosecond laser gasket-drilling device, electrode-deposition device, and the gas-loading device, are also introduced in this article. Finally, we conclude by providing some perspectives on the applications of the DAC in related research fields.

Keywords: high pressure, synergetic measurements, diamond-anvil cell (DAC)

PACS: 07.05.Fb **DOI:** 10.1088/1674-1056/27/7/070701

1. Introduction

Pressure is an important thermal dynamic parameter and can be defined as the force per unit area. As an independent degree of freedom, apart from the temperature and composition, pressure can change the distance between atoms in matter, thus changing the structure and finally affects their properties. When the pressure exceeds 100 bar, it can be considered as a high-pressure condition, which widely exists in the universe, such as in the deep sea, inside the earth, or on other planets. High-pressure research will help us not only gain further insight into the universe but also create new phenomena and materials that have never been observed.

Owing to the continuous development of various pressure devices and probing techniques over the last several decades, high-pressure research has been advanced rapidly. Currently, there are two major high-pressure techniques: the static high-pressure technique and the dynamic high-pressure technique. The static high-pressure technique can maintain the pressure condition significantly longer than the dynamic one and can be easily coupled with other experimental techniques; thus, it has been widely used in the fields of physics, geoscience, chemistry, etc. With the optimized design of the diamond-anvil cell (DAC), the static high pressure can be scaled up to megabars ($>$ 300 GPa), which is almost the same scale as the pressure in the core of the Earth. Furthermore, the dimension of the DAC is a few to tens of centimeters, leading to easy coupling with other sample environments, such as a low/high temperature and high magnetic field. In addition, the diamond, the crucial part of the DAC, is a wide-bandgap insulator with ultralow electrical conductivity even at high temperatures. Diamond exhibits almost 100% transmittance for visible light, infrared (IR) light, and high-energy x-rays and shows strong absorption only in the range of 5–5000 eV (from ultraviolet light to soft x-rays). The combination of its ultralow electron conductivity, high transparency to light, and excellent chemical stability makes diamond a perfect anvil for high-pressure electrical-transport and spectroscopy experiments.[1,2] The combination of various extreme experimental environments (such as high pressure, low/high temperature, and strong magnetic field) with different characterization methods and techniques allows us to observe many fantastic phenomena, such as the near-room temperature superconductivity of H_3S, different stoichiometric sodium chloride, etc.[3–6]

In the High-Pressure Synergetic Measurement Station (HP-SymS), we will develop an integrated user facility with ultrahigh-pressure capacity based on the DAC techniques, up to at least 300 GPa under various extreme conditions. Combined with cryostat and magnet, we will reach a harsh environment of 300 GPa–4.2 K–9 T simultaneously, which is sig-

*Project supported by the National Key R&D Program of China (Grant No. 2016YFA0401503) and the National Natural Science Foundation of China (Grant Nos. 11575288 and 51402350).

†These authors contributed equally to this work.
‡Corresponding author. E-mail: yuxh@iphy.ac.cn
§Corresponding author. E-mail: zhouqiang@jlu.edu.cn

© 2018 Chinese Physical Society and IOP Publishing Ltd

nificant for new physics exploration and benefits condensed-matter physics research, such as the superconductivity, quantum critical behavior, and multifunctionality. Under such a synergetic extreme sample environment, we will be able to study the optical properties via Raman/Brillouin spectroscopy, as well as the electrical-transport properties. Raman/Brillouin spectroscopy probes the molecular dynamics and provides direct information on the inter-atomic interactions, molecular atomic geometries, and structural phase transitions. Measurements of the electrical-transport properties, including the direct-current (DC) resistivity, the Hall effect, and the alternating-current (AC) impedance, can reveal information about the electron–phonon scattering and the electron interactions corresponding to the microscopic lattice structure, spin, and orbital ordering parameters. The simultaneous measurements of the Raman/Brillouin spectroscopy and electrical-transport properties under the synergetic high P-low T-high B condition will help us to gain deep physical insight into the modern physics and even break through the existing physics models and create new theories.

Furthermore, the laser-heating technique will be introduced to the HP-SymS for achieving a high-temperature condition inside the DAC. The target temperature of 3000 K is obtained via double-side laser heating. In the experimental setup, Raman/Brillouin spectroscopy will be the dominant probe to study the structural evolution *in situ*. Under the high-pressure and temperature conditions, we will be able to simulate the earth's core environment and synthesize new phase/materials, providing important implications to the geoscience and high-pressure chemistry.

In the end of this section, we want to emphasize the importance of synergetic high-pressure measurements, which are critical and highly demanded by ultrahigh-pressure experiments. Ultrahigh-pressure experiments are very challenging and expensive. Measurement of various properties requires multiple loadings and consequently consumes diamonds, because ultrahigh-pressure experiments generally involve one-time loading and releasing the pressure usually breaks the diamond anvils owing to the high strain contained. The new synergetic measurements will substantially reduce the cost because we can finish various measurements at the same time with the same pressure in one single-loading. Additionally, it is challenging to calibrate the ultrahigh pressure. It is difficult to achieve exactly the same pressure/temperature condition for different measurements. In traditional multi-measurement experiments, the data are not collected under the same condition, which introduces uncertainty and inconsistency in the data analysis. Fortunately, the HP-SymS solves this problem and will allow researchers to collect reliable and consistent data via a single experiment.

2. Main components of HP-SymS

In the High Pressure Synergetic Measurements Station (HP-SymS) of the Synergic Extreme Condition User Facility (SECUF), there are three primary modules: the sample environments module, the measurements module, and the supporting module, as detailed below.

(I) Sample environments module

a) Ultrahigh-pressure device (DAC)

b) Low temperature–high magnetic field device

c) High-temperature devices: laser heating and resistant heating

(II) Measurements module

a) Electrical transport properties measurements

b) Raman spectroscopy

c) Brillouin spectroscopy

(III) Supporting module

a) Electrode-deposition device

b) Focused ion beam (FIB)/scanning electron microscopy (SEM)

c) Gas-loading device

d) Ruby line

e) X-ray diffraction (XRD) device at high pressure

f) Sample-loading device

g) Gasket-drilling device

h) Gas-membrane controller

As shown in Fig. 1, the sample environment module provides the basic high pressure–low temperature–high magnetic field and the high pressure–high temperature conditions. Under the same conditions, the sample in the synergetic sample environment will be characterized by electrical-transport measurements and Raman/Brillouin spectroscopy simultaneously. The high-pressure experiments require delicate preparation. The supporting module will help users to load DAC samples in a far easier way, simply by clicking a mouse, than manual pressure control based on the digital gas-membrane system.

(I) Sample environments module

a) DAC that generates ultrahigh-pressure condition

In the history of high-pressure science, the DAC can be traced back to the 1950s. It has played a very important role until now and will continue to do so in the future. There are many different kinds of DACs, but their main structures are the same: (1) the anvil/gasket assembly; (2) the backing plates, which might include an alignment mechanism; and (3) the thrust-generating mechanism.[7–9]

The high pressure that a DAC can generate mainly depends on the culet size and designs. A smaller culet yields a higher pressure in the experiment. The culet size varies from tens of microns to a few millimeters according to the target pressure and experimental requirements. DAC with simple flat culets can reach a pressure around 100 GPa. To achieve

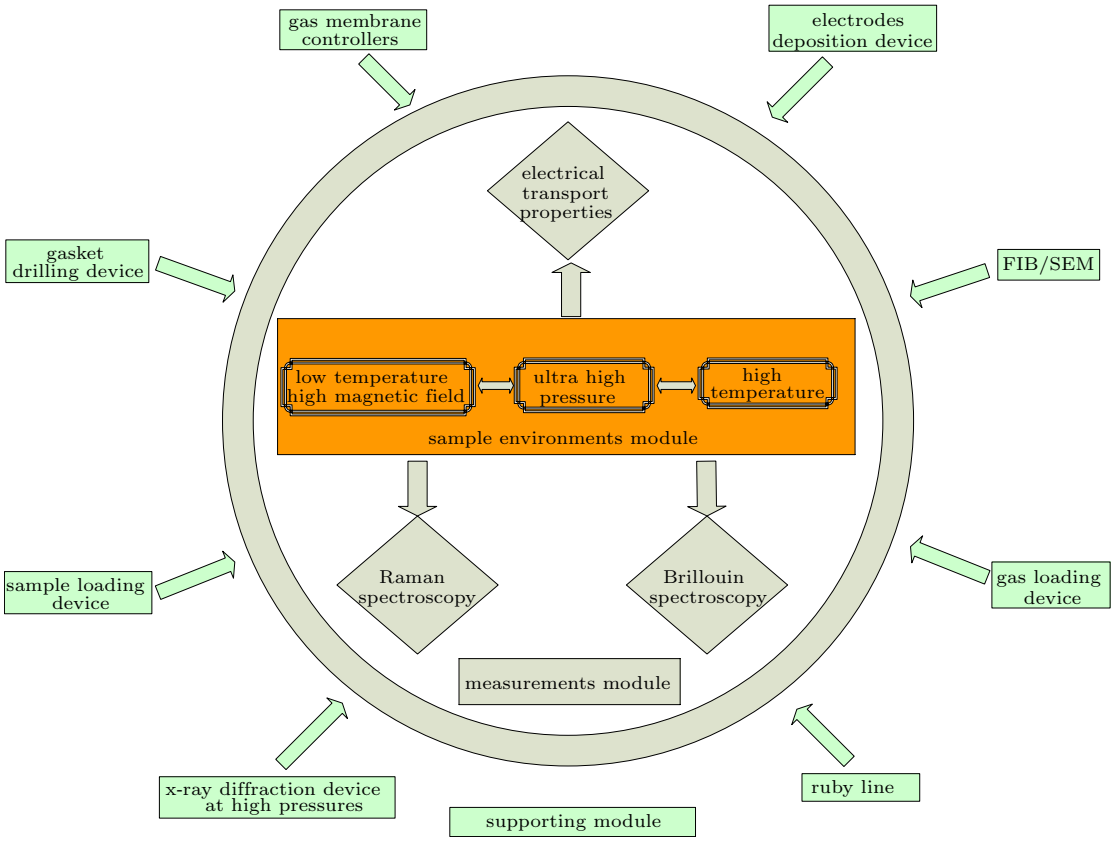


Fig. 1. (color online) Main components of the HP-SymS.

higher pressure, beveled anvils are needed. With a fine-tuned and optimized culet diameter (e.g. 20 μm, as shown on the left side of Fig. 2) and bevel angle, an ultrahigh pressure up to 300–400 GPa is reachable.[10] The behavior of the DAC is investigated up to 400 GPa, which is the accepted pressure limit of a conventional DAC. By using a sub-micrometer synchrotron x-ray beam, double cuppings of beveled diamond anvils were observed experimentally.[11] Recently, an ultrahigh static pressure over 600 GPa was generated using high-strength nano-diamond (as shown on the right-hand side of Fig. 2), but this technique is not robust or reproducible for studies of real samples.[12]

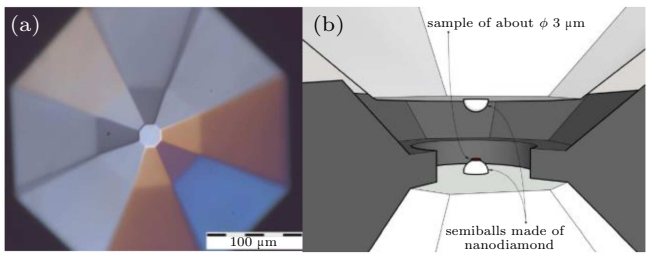


Fig. 2. (color online) (a) Beveled diamond anvils with culet diameters of ∼ 20 μm and (b) the design of the double-stage nano-diamond.[11]

In the HP-SymS, beveled diamond anvils with different culet diameters are provided to attain a high pressure over 300 GPa. Various types of DACs can be selected to satisfy the different demands of users in experiments. For a low-temperature and magnetic environment, nonmagnetic BeCu-DAC can be selected. For a high-temperature environment, a specially designed thermostat DAC is fit, in which a high temperature over 1000 K can be achieved, while the DAC body can be kept at room temperature by using heat insulation and a water-cooling system, as shown in Fig. 3.[10] The gas-membrane DAC, which can ensure both the accuracy of pressure loading and the safety of users via remote control of the gas loading, is another option for high-temperature experiments. All DACs in the HP-SymS can reach a high pressure over 100 GPa.

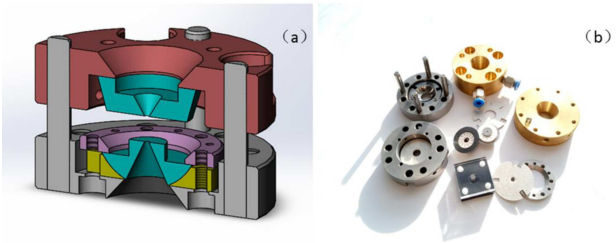


Fig. 3. (color online) DAC combined with water-cooling system for high-temperature experiments.[10]

b) Low temperature–high magnetic field device

Currently, there are mainly two different types of DAC cryostat designs. One is the open-cycle cryostat using liquid He (LHe). It can reach a very low temperature, e.g., 2 K, via

depressurization. However, this type of DAC cryostat consumes a large amount of He, and it is hard to open optical windows for spectroscopy experiments. Another option is the He-free cryostat, which cools the DAC using a cryocooler. However, the vibration from the cryocooler usually affects the optical experiments severely. For the high pressure–low temperature spectroscopy experiments in HP-SymS, it is important to develop a He-free cryostat with low vibration.

In the HP-SymS, we collaborated with Janis and Physike Technology Co., Ltd and developed a new He-free, low vibration, closed cycled cooler system (recirculating He gas cooler) based on Janis ST-500. As shown in Fig. 4, this cryostat employs recirculating He gas as a direct replacement for LHe and cool continuous flow cryostats without the use of LHe. As shown in Fig. 4, the He gas passes through a series of heat exchangers on the cryocooler and then flows through the integrated vacuum insulated transfer line into the cryostat. After the sample is cooled, the gas is returned to the cryocooler for re-cooling and continues circulating. In order to achieve lower base temperature, this recirculating He gas cooler contains a Joule–Thomson (JT) valve, which allows the JT effect to take place after the needle valve orifice and can be implemented with a throttle valve. This process can make the temperature of the condensed helium liquid lower. The liquid is then depressurized by an external pump and reaches its minimum temperature. This provides a cost-effective platform with low vibration and low drift. The base temperature can reach below 3.5 K using a 1.5 W@4.2 K pulse tube cooler. The nominal vibration amplitude is within ±5 nm, and the positional drift is within 10 nm@5 min.

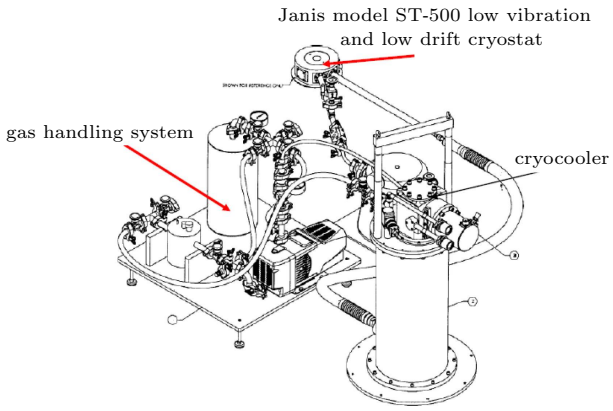


Fig. 4. (color online) Sketch of the recirculating He gas cooler plus ST-500 cryostat.

In order to carry on high pressure–low temperature–high magnetic field microscopy experiments, we apply a compact superconducting magnet with a large room temperature (RT) bore size from Cryomagnetics. As shown in Fig. 5, the thickness of 9 T compact superconducting magnet is only 9.2″ with a 3.28″ RT bore, which allows the insertion of a microscopy cryostat with a snout into the magnetic-field center to conduct high pressure–low temperature–high magnetic field microscopy experiments.

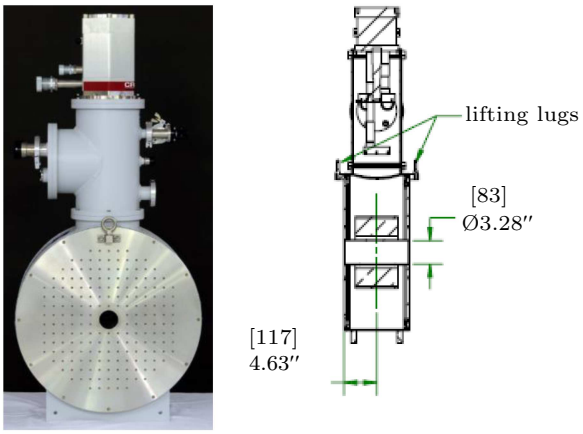


Fig. 5. (color online) Compact 9 T cryogen-free superconducting magnet with 3.28″ RT bore size.

Figure 6 shows a sketch of the high pressure–low temperature–high magnetic field microscopy system matching with a Raman spectrometer. This system includes ST-500 microscopy cryostat with a snout for mounting the membrane-driven DAC, a recirculating He gas cooler, a compact superconducting magnet, a magnet support, and a cryostat translation stage, which can match with Raman spectrometer through special design light extension tube.

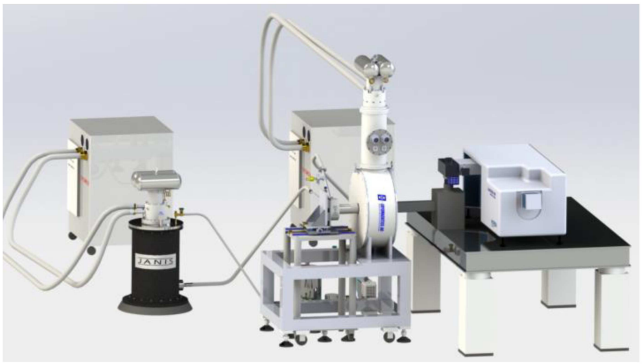


Fig. 6. (color online) Sketch of high pressure–low temperature–high magnetic field microscopy system matching with Raman spectrometer.

c) High-temperature devices: laser heating and resistant heating

The high-temperature technique combined with the DAC mainly includes two methods: laser heating and resistant heating. The idea of laser heating for the DAC was proposed by Taro Takahashi and William A. Bassett about 60 years ago, and initial laser-heating experiments on silicates were reported a few years later. Currently, laser heating in DACs can be coupled with other *in situ* spectroscopy measurements or synchrotron radiation facilities and has become a powerful experimental technique for studying a broad range of material properties over a wide *P*–*T* field. Continuous-wave laser heating

provides better system stability which is essential for long-term heating and reaching a high temperature for overcoming kinetic barriers to phase transition and for enabling the synthesis of new materials. The most commonly used laser-heating facilities employ a continuous-wave near-IR laser as the energy source. Two favorable choices are the CO_2 laser (10.6 μm) and solid-state lasers (∼ 1 μm, e.g., YAG, YLF, fiber laser). In recent years, modulated pulse laser heating is developed and used for increasing high pressure research. As the heating duration is significantly reduced, the thermally activated chemical reaction is effectively suppressed, and the possibility of achieving high-temperature conditions increases; thus, modulated pulse laser heating is useful for studies on phase-transition dynamics and investigations of various physical and chemical phenomena occurring in short time scales.

The laser-heating system in this station is integrated with a Raman/Brillouin scattering spectrum system, and a continuous-wave solid-state laser with a wavelength of ∼ 1 μm is employed as the energy source. The CO_2 laser radiation can be absorbed effectively by most optically transparent materials and is a good choice for Brillouin-scattering experiments in the forward scattering geometry, as the samples are optically transparent. However, the stability of the CO_2 laser is inferior to that of the solid-state IR laser, and the setup of the whole system path is complicated in order to avoid absorption by optical glasses. Double-sided laser-heating paths and *in situ* double-sided temperature-measurement paths are included in the system, and two solid-state IR lasers are used for heating the DAC from each side independently. The path of each laser beam includes a laser-beam expander, a dichroic mirror (DM), an apochromatic objective lens, a Ag coating-protected reflecting mirror, dichroic mirror, and filters for focusing the laser beam and collecting thermal radiation. The temperature is measured by fitting the thermal-radiation spectrum of the sample to a grey body curve, and the target temperature of the laser-heating system is $T > 3000$ K.

For the resistant heating, it has been well developed and commercialized. The only concern is the oxidation of diamond at high-temperature conditions in the air; thus, both the DAC and the resistant-heating oven should be protected by the Ar atmosphere.

(II) Measurements module

a) Electrical transport properties measurements

The study of the electrical-transport properties of condensed matter is an important issue in high-pressure science. Multiple solutions have been integrated into the HP-SymS for the study of the electrical properties under an ultrahigh pressure with DACs, including the *in situ* DC resistance (resistivity), Hall effect, and AC electrochemical impedance spectroscopy measurements. Thus, the pressure-induced metallization and superconducting transition, as well as the evolution of the charge-carrier behaviors, dielectric properties, and grain-boundary effects, can be revealed.

DC resistance (resistivity) measurements Using the measurement station, the DC resistance can be measured for liquid (including gas), powder, or single crystal samples. Two different forms of the electrode can be chosen according to the state of the samples (Fig. 7). The first is metallic wires that must be placed manually in the DAC sample chamber and can provide good contact for single crystal samples.[13] The other is integrated thin-film electrodes on diamond anvils. Because the thin-film electrodes have a predesigned shape and position and remain unchanged under a high pressure, the resistivity value can be obtained more precisely via finite-element analysis of the electric field.[14,15]

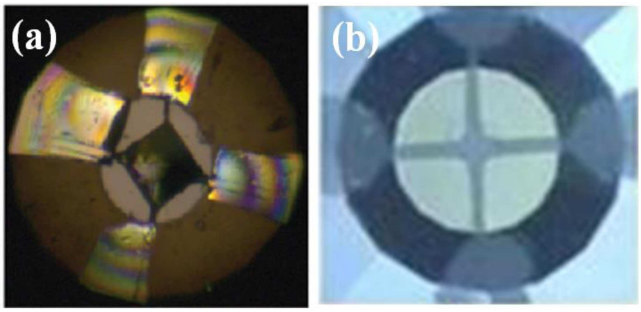


Fig. 7. (color online) Electrodes on the diamond anvil: (a) wire electrodes, (b) thin-film electrodes.[13]

Hall-effect measurements Owing to the benefit of the advanced integration technique of thin-film electrodes on DACs, the HP-SymS can perform more accurate Hall-effect measurements with a strictly symmetrical van der Pauw electrode configuration.[16] The station can provide a Hall-effect measurement environment for samples in the resistance range of 0.5 mΩ–10 MΩ in the standard mode and 10 kΩ–50 GΩ (8 GΩ) in the high-resistance DC (AC) mode, in the carrier-concentration range of 8×10^2–8×10^{23} cm^{-3}, and in the mobility range of 10^{-3}–10^6 cm^2/V·s. The obtained strongest magnetic field is 1.67 T (DC) and 1.18 T (AC) at ambient temperature.

AC electrochemical impedance spectroscopy measurements Impedance spectroscopy measures the dielectric properties of a medium as a function of the frequency. It is based on the interaction of an external field with the electric dipole moment of the sample, which is often expressed by permittivity. It is also an experimental method for characterizing electrochemical systems.

In the HP-SymS, the dipolar relaxation, ionic relaxation, and dielectric relaxation behaviors under a high pressure can be studied via impedance spectroscopy.[17–20] The AC impedance spectrometer can provide a wide converted

frequency range of 10 μHz–32 MHz and measure a high impedance over 100 TΩ.

b) Raman spectroscopy

High-pressure Raman investigation plays an important role in high-pressure physics and geophysics, revealing the vibrational, electronic, and structural properties of materials. Raman spectroscopy has become an indispensable tool for high-pressure studies. The confocal Raman microscope obtains detailed images and allows measurements of very small samples in DACs under ultrahigh pressures (exceeding 300 GPa). By using the double-subtractive configuration of a triple system or a Bragg notch filter, it is possible to access very low frequencies even below 10 cm^{-1}. The ultralow-frequency Raman spectra provide important information regarding the conformational changes or subtle changes of the lattice structure, for example, in graphene, transition-metal dichalcogenides, or other semiconductors. The optimized spectroscopy can also provide a high resolution (up to 0.15 cm^{-1}), which is important for analysis of the crystallinity, polymorphism, and strain, along with other band analyses. One set of Raman spectroscopy experiments involving multiple excitations with different laser wavelengths and multiple mounted detectors enables measurements covering the UV–vis to NIR bands. Such performance opens up other spectroscopic techniques, such as UV Raman spectroscopy, resonance Raman spectroscopy, and photoluminescence spectroscopy, allowing detailed sample characterization of various materials. Raman spectroscopy combined with DAC was conjunctive to the laser heating optic block to provide *in situ* vibrational information under high pressure and high temperature environments. In HP-SymS, the Raman spectroscopy was also conjunctive to cryostats containing DACs for realizing *in situ* high-pressure and low-temperature measurements. A practically non-magnetic objective lens will be used for collecting scattered light under a magnetic field and low-temperature conditions (9 T, 4.2 K).

c) Brillouin spectroscopy

Brillouin spectroscopy is able to determine the acoustic velocities of numerous crystalline solids, amorphous glasses, polymers, and liquids. The target signal is due to the inelastic scattering of light caused by spontaneous collective motions of particles in materials in the frequency range of 0.01 to 10 GHz. Owing to the small frequency shifts of the thermal acoustic phonons measured in Brillouin scattering, the traditional grating monochromator used for obtaining Raman spectrographs cannot provide a high resolution; rather, Fabry–Perot interferometers are used. A Fabry–Perot interferometer consists of two flat-plane mirrors mounted parallel to one another with high accuracy. It behaves as a comb filter, transmitting a theoretically infinite set of wavelengths spaced by a constant interval. However, a single Fabry–Perot interferometer does not provide enough contrast to measure the Brillouin scattering. To improve the contrast and extend the free spectral range of the spectrometer, a multi-pass tandem configuration ($3+3$ pass, Fig. 8) was used so that the instrumental contrast was enhanced to 10^{15}.

Besides, the new TFP-2 HC interferometer enables optional excitation between 473 nm and 532 nm, which is achieved by changing mirrors allowing 532 nm or 473 nm wavelength accordingly. The detector for a Brillouin scattering spectrometer is also optional, depending on the trade-off between a high efficiency in the energy range of interest and a good signal-to-noise ratio. For large, intense scattering samples, photomultiplier tubes (Laser Components Count-10B) were sufficient for obtaining the best signal-to-noise ratio, whereas for small samples or measurements under ultrahigh pressure and temperature conditions producing extremely weak Brillouin signals, the specially selected Hamamatsu H10682 detector with modification achieved a maximum dark count of 2 cts/s at room temperature.

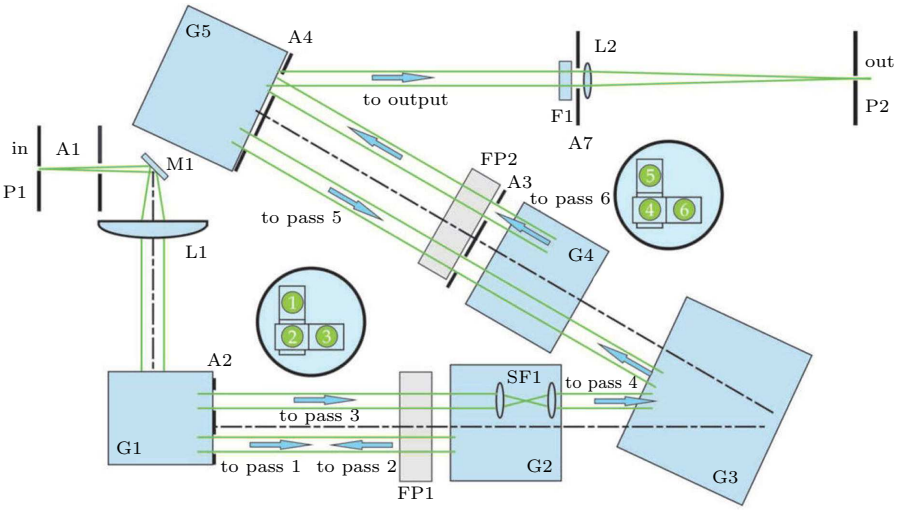


Fig. 8. (color online) $3+3$ pass Fabry–Perot interferometer in the "tandem" mode.

Brillouin scattering can be combined with DACs and a high-temperature system, as a very small sample is sufficient for measurement. The Brillouin-scattering measurement includes different geometries of the incident and scattered light paths, such as the normal geometry (90°), backscattering geometry (180°), tilted backscattering geometry, and forward symmetric geometry, which are typically used for transparent samples in DACs. The symmetric geometry of the laser path for Brillouin and long-focal length achromats used for collecting scattered signals ensure that there are no conflicts of the laser paths or occupations with the Raman scattering or laser-heating parts.

(III) Supporting module

a) Electrode-deposition device

The HP-SymS uses a magnetic-sputtering device to deposit metallic thin-film electrodes on the DAC. The device consists of a vacuum chamber, a vacuum pumping system, a target, a DC/radiofrequency (RF) current source, a heatable wafer stage, a gas circuit, a water-cooling system, and an electronic control system. Under operation in an Ar atmosphere and the RF mode, nonmagnetic metals, alloys, and dielectric materials can be sputtered. In the DC mode, the sputtering of magnetic metals such as Fe, Co, and Ni is available. If another gas, such as O_2 or N_2, is injected into the device together with Ar, reactive magnetic sputtering can be fulfilled, and oxide and nitride thin films can be obtained.

b) FIB/SEM

This SEM with FIB capability is mainly used to prepare high-quality, high-pressure diamond anvils and gaskets. For the ultrahigh-pressure experiment, the sample chamber can be very small, even smaller than 20 μm. In addition, it is necessary to shape the diamond anvils. Traditional laser drilling and machine drilling can provide good gaskets for a general high-pressure experiment. However, for an ultrahigh-pressure measurement ($>$ 200 GPa), a higher-quality sample chamber is needed to maintain the pressure stability. The FIB provides an accurate method for obtaining the required round-shape sample chamber hole without serious edge damage. For the anvil processing, traditional milling cannot control the shape at the microscale. With the help of the SEM imaging function and advanced FIB cutting function, we can shape the anvils via pre-design. In addition, the samples recovered from the high-pressure experiments can be processed by this FIB/SEM instrument for further characterizations, such as transmission electron microscopy.

c) Gas-loading device

In the DAC high-pressure experiments, the pressure media is very critical for the hydrostatic condition. For most liquid pressure media (for example, silicon oil and methanol/ethanol/water mixtures), the hydrostatic condition can only reach 12 GPa. However, if we load Ne or He gas into the DAC as the pressure media, the hydrostatic condition can reach 25 or 50 GPa. Even if the Ne or He gas solidifies, the hydrostatic condition is still much better than those of silicon oil and methanol/ethanol/water mixture. In addition, the gas-loading device is necessary for investigating the high-pressure gas behavior, e.g., the metallic H, or the high-pressure chemical reactions. The core components of the gas-loading system are the gas compressor and the gas cylinder for the DAC. Fortunately, both of these are commercially available. Figure 9 shows the gas-loading device, which contains a high-pressure gas compressor (maximum output gas pressure of 200 MPa) and the gas cylinder for the DAC.



Fig. 9. (color online) (a) Gas-loading device, (b) the high-pressure gas compressor (maximum output gas pressure of 200 MPa), and the gas cylinder for the DAC.

d) Ruby line

For pressure calibration in the low-pressure range ($<$ 80 GPa), measuring the ruby photoluminescence is still the most popular method in a high-pressure field, because ruby is very sensitive to the external pressure and allows fast measurement of the pressure. This can be accomplished using a well-developed device, which we will build in this station according to an existing design. For pressure calibration in high-pressure range ($>$ 80 GPa), the Raman peak shift of diamond is applied.

e) XRD device at high pressure

High-pressure structural transition is one of the most important research topics in high-pressure science. Normally, the structure is characterized through *in situ* high-pressure synchrotron experiments. However, the synchrotron sources in the world are very limited, and high-pressure beamlines are highly demanded. It is not always easy to be granted beam time for high-pressure experiments. Currently, owing to the development of XRD technology, it is possible to conduct high-pressure XRD with DACs in the laboratory. Figure 10(a) shows the XRD facility integrated with a DAC, and figure 10(b) shows an obtained diffraction pattern. The typical data-collection time is approximately 30 min for the metal powders.

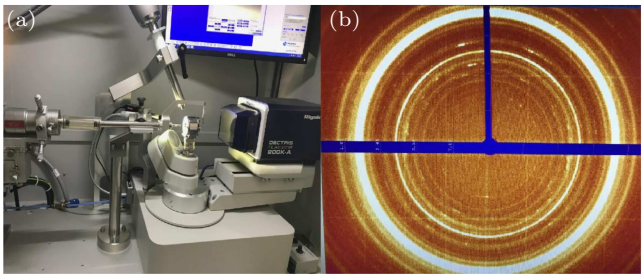


Fig. 10. (color online) (a) XRD machine integrated with a DAC, and (b) a corresponding diffraction pattern.

f) Sample-loading device

For some new users of the DAC, sample loading at the microscale is very challenging. The commercial device helps beginners to load samples easily into the DAC.

g) Gasket-drilling device

At present, the methods for drilling gaskets mainly include mechanical drilling, electrical-discharge machining, and laser drilling. Laser drilling is superior to the other methods with regard to machining quality and accuracy; therefore, it has become the mainstream method for drilling DAC gaskets. Conventional laser-drilling machines mainly use picosecond or nanosecond lasers, and owing to the thermal effect, there is a 10–20 μm hot-melt zone around the hole, which is soft and cannot hold the pressure very well, especially with gas as the pressure medium. Although ordinary laser drills are sufficient for routine high-pressure experiments ($<$ 150 GPa, usually with a drill diameter larger than 50 μm), they can no longer satisfy the demand for experiments over 300 GPa, because the mesa of the secondary chamfered is only 20 μm, and the size of the hole is usually 5–10 μm.

In the HP-SymS, a new type of femtosecond laser micromachining system was developed by our team at the Institute of Physics, the Chinese Academy of Sciences in collaboration with Beijing Rui Ke Tai Optoelectronic Technology Co., Ltd. The new system uses a laser with a pulse width of 400 fs and can achieve minimal hole machining of about 3 μm. The hot-melt zone around the hole is only 1–2 μm. The system allows the machining of non-metals and even transparent materials, for example, cubic boron nitride or sapphire inline gaskets. Furthermore, the system can perform micro-and nano-machining of various metal and non-metal materials through two-dimensional (2D) graphics prepared by software.

As shown in Fig. 11, the system includes the following main components: femtosecond lasers, a beam-shaping system, imaging setup transmission, a laser-processing objective, and a multidimensional motion-control system.

In the system, we use a Spirit-HE femtosecond laser with an average power of 16 W, a single pulse energy greater than 120 μJ, and a pulse width less than 400 fs. The extremely high peak power and narrow pulse width produce very weak laser ablation during the machining of various materials. The beam-shaping system is used to optimize the beam quality of the femtosecond laser and allows the laser to be focused onto smaller spots. The guided-light imaging system is shown in Fig. 12. It includes the following: a charge-coupled device (CCD) camera, a filter, an imaging lens system, a beam splitter (BS), a light-emitting diode (LED), and a DM. The main function of the guided-light imaging system is to introduce the laser beam from the beam-shaping system into the laser-processing objective lens. Simultaneously, coaxial lighting and real-time monitoring of the workpieces are performed.

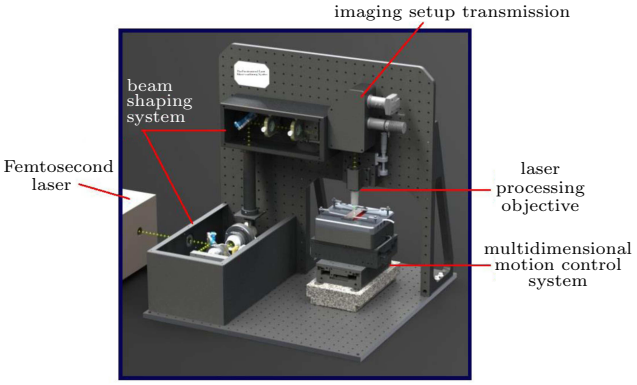


Fig. 11. (color online) Femtosecond laser micromachining system.

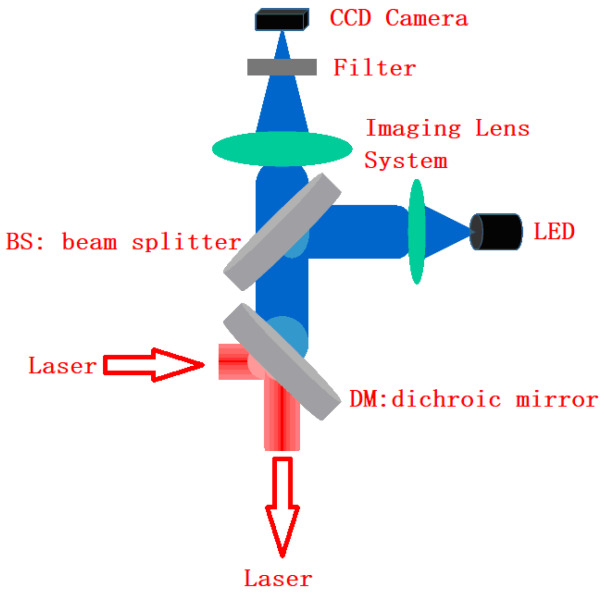


Fig. 12. (color online) Guided-light imaging system.

The laser-processing objective system uses a 50× infinity field achromatic objective lens, which is a special optical design with a large numerical aperture. The laser-processing objective focuses the laser beam onto the samples (gasket), whose positions are precisely controlled via the multidimensional motion-control system.

3. Recent research progresses with DAC

3.1. Conventional superconductivity at 203 K at high pressures in the sulfur-hydride system

Although a very high superconducting transition temperature, T_c, is observed in the copper-oxide system, 133 K at the ambient pressure[21] and 164 K at high pressures,[22] the prospects for achieving higher transition temperatures via this route are not clear, because these materials are not conventional superconductors, and the nature of superconductivity is not fully understood. In contrast, it is very likely to achieve T_c of much higher in the system based on the Bardeen–Cooper–Schrieffer theory of conventional superconductivity as long as the materials have a favorable combination of high-frequency phonons, strong electron–phonon coupling, and a high density of states, which can in principle be fulfilled for metallic hydrogen and covalent compounds dominated by hydrogen. Recently, the superconducting transition at a record high temperature of 203 K was detected in the H-S system at 155 GPa via measurement of the *in situ* resistance and magnetic properties in a DAC, as shown in Fig. 13.[5] Theoretical calculations and high-pressure XRD experiments have shown that the high superconducting critical temperature over 200 K results from the decomposition of H_2S into elemental sulfur and H_3S.[4,23] *In situ* AC magnetic-susceptibility measurements on compressed H_2S were also performed in the DAC. It was shown that superconductivity suddenly appears at 117 GPa and that T_c reaches 183 K at 149 GPa before decreasing monotonically with a further increase in pressure.[24]

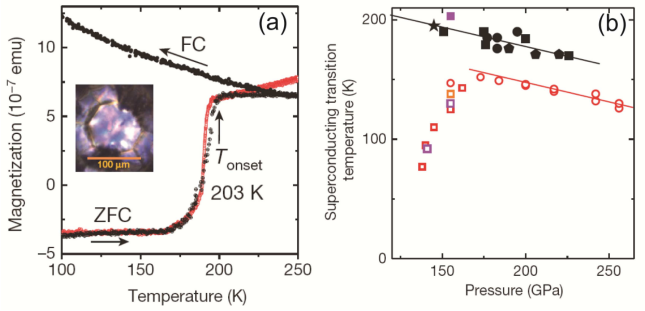


Fig. 13. (color online) Superconductivity in H_3S at high pressures. (a) Temperature dependence of the magnetization of sulfur hydride at a pressure of 155 GPa in the zero-field cooled and 20-Oe field-cooled modes (black circles). The onset temperature is 203 K. (b) Dependence of T_c on the pressure. The open colored points correspond to sulfur deuteride, and the filled points correspond to sulfur hydride. The data represented by the magenta points were obtained via magnetic-susceptibility measurements (from Ref. [5]).

3.2. Pressure-induced isostructural phase transition and correlation of FeAs coordination with superconducting properties of 111-Type $Na_{1-x}FeAs$

Other than the conventional superconductivity, the high pressure is an effective approach for searching novel classes of unconventional superconductors, such as the heavy-fermion, organic, cuprates, and the iron-based superconductors.

Compared with the chemical pressure induced by doping, the physical high pressure condition introduced by the DAC provides a clean and direct method for tuning the superconductivity. In the NaFeAs system, the effect of pressure on the superconductivity of "111"-type $Na_{1-x}FeAs$ is investigated via temperature-dependent electrical-resistance measurements in a DAC. The superconducting transition temperature (T_c) increases from 26 K to a maximum of 31 K as the pressure increases from the ambient pressure to 3 GPa. Further increasing the pressure suppresses T_c drastically. The behavior of pressure-tuned T_c in $Na_{1-x}FeAs$ differs significantly from that in Li_xFeAs, although these materials have the same Cu_2Sb-type structure. The effect of the pressure on the crystalline structure and superconducting transition temperature (T_c) of the 111-type $Na_{1-x}FeAs$ system is studied using *in situ* high-pressure synchrotron x-ray powder diffraction and DAC techniques, as shown in Fig. 14. A pressure-induced tetragonal-to-tetragonal isostructural phase transition was observed. The systematic evolution of the $FeAs_4$ tetrahedron as a function of the pressure based on Rietveld refinements of the powder XRD patterns was obtained. The nonmonotonic T_c(P) behavior of $Na_{1-x}FeAs$ is found to correlate with the anomalies of the distance between the anion (As) and the Fe layer, as well as with the bond angle of As–Fe–As for the two tetragonal phases. This behavior provides the key structural information for understanding the origin of the pressure dependence of T_c for 111-type iron-pnictide superconductors. A pressure-induced structural phase transition is also observed at 20 GPa.

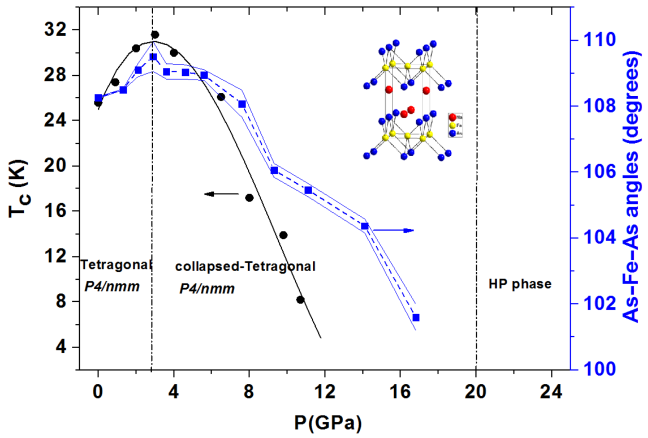


Fig. 14. (color online) Effect of the pressure on the crystalline structure and superconducting transition temperature (T_c) of the 111-type $Na_{1-x}FeAs$ system.[26]

Our results indicate the non-monotonic relation between T_c(P) and change of the anion height from iron layer and the As–Fe–As bond angle with maximum T_c correlating both with

regular $FeAs_4$ tetrahedron and the optimal distance between arsenic element and iron layer.[25,26]

3.3. High pressure-induced phase transition and equation of state

High pressure is a very effective way to change the distance between atoms and consequently change the structure of matter. It was predicted that condensed matter undergoes five phase transformations on average upon compression to 100 GPa. The structure transformation might be accompanied by important property evolution. In addition, for geoscience, it is very important to derive the equation of state for minerals under high-pressure conditions, which corresponds to the theoretical density and affects the earth plate movement, mantle convection, and geomagnetic reversal. In condensed-matter physics, applying a high pressure is a very effective method for finding the strengthening phase, as the atomic arrangement in the high-pressure condition is more effective than that in ambient conditions. For superhard materials, the bulk modulus derived from the high-pressure equation of state is one of the most important parameters. It is defined as the ratio of the infinitesimal pressure increase to the resulting relative decrease of the volume, more specifically, the ratio of the resistance to the compressibility. Over the last decade, researchers have directed considerable effort towards the study of transition-metal nitrides and borides because they possess remarkable electrical conductivity and magnetic properties, combined with high hardness. For example, we studied numerous novel tungsten-nitride products that exhibit elastic properties rivaling or even exceeding those of cubic-BN.

To derive the high-pressure equation of state for the W-N system, including h-W_2N_3, r-W_2N_3, c-W_3N_4, and δ-WN, we conducted high-P synchrotron x-ray experiments using a DAC. The powder nitrides were loaded into the sample hole in the Re gaskets with He as the pressure-transmitting medium in all experimental runs. The samples in the DAC were compressed to pressures reaching 50 GPa at room temperature. The collected diffraction data were analyzed by integrating 2D images as a function of 2θ using the program Fit2D to obtain conventional, one-dimensional diffraction profiles. The pressures in all of the experiments were determined via the ruby scale. The refined lattice parameters are fitted to the third-order Birch–Murnaghan equation of state:

$$P = 3/2B_0\left[(V/V_0)^{-7/3} - (V/V_0)^{-5/3}\right] \times\left\{1 - 3/4(B'-4)\left[1-(V/V_0)^{-2/3}\right]\right\}. \quad (1)$$

The definitions of P, B_0, B', V, and V_0 are presented in Ref. [27], and the data fittings are shown in Fig. 15. The insets show the normalized pressure (F) as a function of the Eulerian strain (f). The B_0 and B' values determined from the $F-f$ plots for all these nitrides are in excellent agreement with those obtained from the third-order Birch–Murnaghan equation of state. The determined bulk moduli (B_0) from both the experiments (376 GPa) for c-W_3N_4 and (391 GPa) for WN are comparable to that of cubic boron nitride (c-BN). For h-W_2N_3, although it is elastically more compressible than c-W_3N_4 and WN, the experimentally determined B_0 (331(12) GPa) is still within $\sim 10\%$ of that of c-BN. These exceptional properties indicate the tested materials are potential candidates for novel hard or superhard materials.[28]

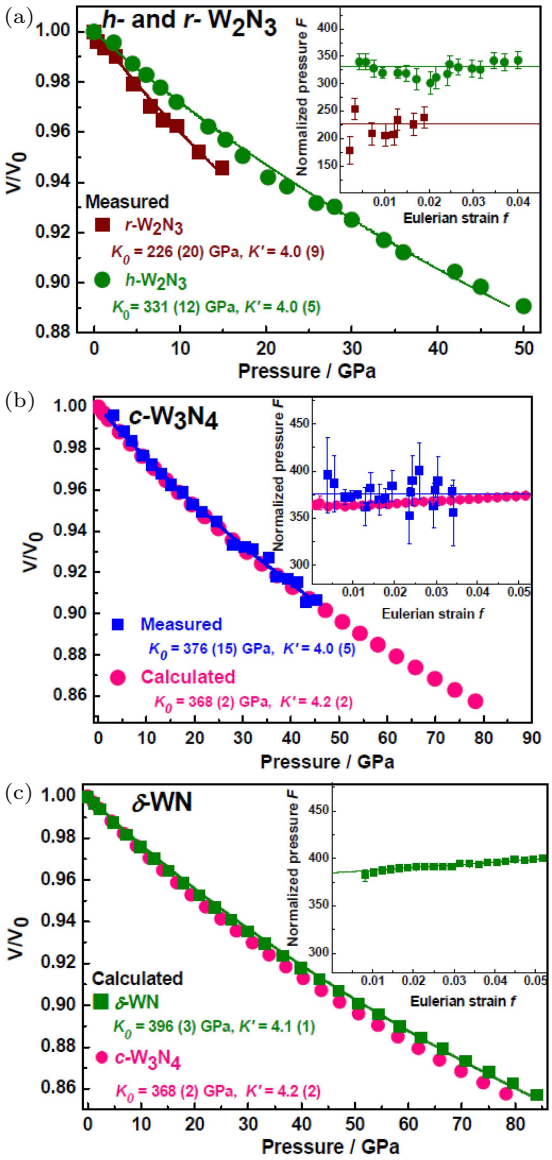


Fig. 15. (color online) Volume–pressure data for (a) h-W_2N_3, r-W_2N_3, (b) c-W_3N_4, and (c) δ-WN.[28]

In addition to the transition metal nitride, we studied boride ZrB_{12}, which exhibits a very symmetrical cubic crystal structure. The phase stability and the compressibility of

ZrB_{12} were investigated via synchrotron XRD in a DAC.[29] The cubic ZrB_{12} was structurally stable up to 43 GPa, and no phase transition was observed. The bulk modulus, B_0, of ZrB_{12} was calculated by fitting the derived pressure–volume data to the second order Birch–Murnaghan equation of state. A B_0 value of 221 (8) GPa at $B' = \partial B/\partial P \approx 4$ was obtained. Interestingly, this value for ZrB_{12} is slightly lower than that for B_6O, $B' = 270$,[30] but significantly lower than those for ReB_2, WB_4, and CrB_4 with a lower concentration of B, because the bulk modulus is mainly attributed to the valence-electron density of transition metals. Although ZrB_{12} has a relatively low elastic bulk modulus, it exhibits hardness rivaling or even exceeding that of the aforementioned borides, because the hardness ultimately measures the plastic deformation under indentations.[29]

Previously, the high-pressure phase transition and equation of state were determined via high-pressure synchrotron XRD experiments. Now, using the modern XRD machine, we can conduct high-pressure XRD in our high-pressure lab.

3.4. Different stoichiometries of sodium chlorides synthesized under high-pressure conditions

With the electron configurations of $3S^1$ for Na and $3S^2P^5$ for Cl, the simple table salt NaCl is the only known stable phase of Na and Cl under ambient conditions. However, under high-pressure conditions, different stoichiometries of NaClx can be adopted, as revealed by Zhang *et al.*[6] According to thermotical predistortions, compounds such as Na_3Cl, Na_2Cl, Na_3Cl_2, $NaCl_3$, and $NaCl_7$ can be stable and have unusual bonding and electronic properties under the high-pressure condition.

To verify these predictions, high-pressure experiments using a DAC coupled with the laser-heating technique were conducted. In a Cl-rich system, two stacked NaCl thin (5–8 μm) plates were loaded into the Re gasket, and the rest of the cavity was cryogenically filled with molecular chlorine. In a Na-rich system, a small piece of Na was loaded between two thin NaCl plates positioned on each diamond anvil in the DAC. Then, the samples in DAC were cocked through double-sided laser heating to 2000 K at 55–80 GPa, and the temperature was determined spectroradiometrically.

XRD measurements of Na_3Cl and $NaCl_3$ synthesized at high pressures indicate new Bragg peaks after laser heating. In the case of Cl-rich materials with pressure above 60 GPa, these Bragg peaks can be indexed either to the cubic $NaCl_3$ unit cell or to a mixture of the cubic and orthorhombic *Pnma* $NaCl_3$ unit cells. With the pressure decreasing below 54 GPa, after laser heating, only the peaks of orthorhombic $NaCl_3$ are present in the XRD patterns (Fig. 16). The case for the Na-rich material is similar but less complex. XRD patterns of the samples laser-heated above 60 GPa indicate new Bragg peaks that can be indexed to a tetragonal $P4/mmm$-Na_3Cl unit cell over the whole pressure range of this study.

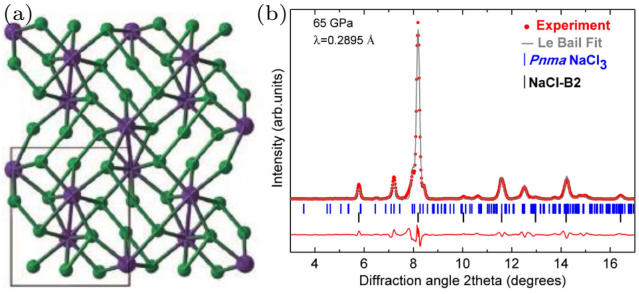


Fig. 16. (color online) (a) Crystal structures of *Pnma*-$NaCl_3$ and (b) the diffraction pattern after laser heating.[6]

4. Conclusion and perspectives

In conclusion, we will develop a set of high pressure–low temperature–high magnetic field and high pressure–high temperature sample environments, based on which conduct the electronical transport properties and Raman/Brillouin spectroscopy measurements simultaneously in the High Pressure Synergetic Measurements Station (HP-SymS) of the Synergic Extreme Condition User Facility (SECUF). By using this station, we will be able to achieve ultrahigh pressure conditions $\sim$ 300 GPa and explore new phenomena and theories in high-pressure science. Once the station is constructed, it will be opened to all users in the world. We will also offer professional assistance to users who are unfamiliar with DAC techniques.

References

[1] Loveday J 2012 *High-Pressure Physics* (Boca Raton: CRC Press)
[2] Mao H K, Chen B, Chen J, Li K, Lin J F, Yang W and Zheng H 2016 *Matter Radiat. At. Extremes* **1** 59
[3] Li Y, Hao J, Li Y and Ma Y 2014 *J. Chem. Phys.* **140** 174712
[4] Duan D F, Liu Y X, Tian F B, Li D, Huang X L, Zhao Z L, Yu H Y, Liu B B, Tian W J and Cui T 2015 *Sci. Rep.* **4** 6968
[5] Drozdov A P, Eremets M I, Troyan I A, Ksenofontov V and Shylin S I 2015 *Nature* **525** 73
[6] Zhang W, Oganov A R, Gancharov A F, Zhu Q, Boulfelfel S E, Lyakhov A O, Stavrou E, Somayazulu M, Prakapenka V B and Konopkova Z 2013 *Science* **342** 1502
[7] Jayaraman A 1983 *Rev. Mod. Phys.* **51** 65
[8] Funamori N and Sato T 2008 *Rev. Sci. Instrum.* **79** 053903
[9] Zsolt J, Hyunchae C, Ken V and William J E 2013 *Rev. Sci. Insrum.* **84** 095114
[10] Mao H K, Chen X J, Ding Y, Li B and Wang L 2018 *Rev. Mod. Phys.* **90** 015007
[11] Li B, Cheng J, Yang W G, Wang J Y, Yang K, Xu R Q, Liu W J, Cai Z H, Chen J H and Mao H K 2018 *P. Natl. Acad. Sci. USA* **115** 1713
[12] Dubrovinskaia N, Dubrovinsky L, Solopova N A, Abakumov A, Turner S, Hanfl, M, Bykova E, Bykov M, Prescher C, Prakapenka V B, Petitgirard S, Chuvashova S, Gasharova B, Mathis Y L, Ershov P, Snigireva I and Snigirev A 2016 *Sci. Adv.* **2** e1600341
[13] Ke F, Dong H N, Chen Y B, Zhang J B, Liu C L, Zhang J K, Gan Y, Han Y H, Chen Z Q, Gao C X, Wen J S, Yang W G, Chen X J, Struzhkin V V, Mao H K and Chen B 2017 *Adv. Mater.* **29** 1701983
[14] Han Y H, Gao C X, Ma Y Z, Liu H W, Pan Y W, Luo J F, Li M, He C Y, Huang X W and Zou G T 2005 *Appl. Phys. Lett.* **86** 064104

[15] Gao C X, Han Y H, Ma Y Z, White A, Liu H W, Luo J F, Li M, He C Y, Hao A M, Huang X W, Pan Y W and Zou G T 2005 *Rev. Sci. Instrum.* **76** 083912
[16] Li Y Q, Gao Y, Han Y H, Liu C L, Peng G, Wang Q L, Ke F, Ma Y Z and Gao C X 2015 *Appl. Phys. Lett.* **107** 142103
[17] Wang Q L, Song D D, Jiao H, Liu C L, Wang W J, Han Y H, Ma Y Z and Gao C X 2017 *Appl. Phys. Lett.* **111** 152903
[18] Wang J, Zhang G Z, Liu H, Wang Q L, Shen W S, Yan Y L, Liu C L, Han Y H and Gao C X 2017 *Appl. Phys. Lett.* **111** 031907
[19] Yan H C, Ou T J, Jiao H, Wang T Y, Wang Q L, Liu C L, Liu X Z, Han Y H, Ma Y Z and Gao C X 2017 *J. Phys. Chem. Lett.* **8** 2944
[20] Yan J J, Ke F, Liu C L, Wang Q L, Zhang J K, Wang L, Peng G, Han Y H, Ma Y Z and Gao C X 2015 *Phys. Chem. Chem. Phys.* **17** 26277
[21] Schilling A, Cantoni M, Guo J D and Ott H R 1993 *Nature* **363** 56
[22] Gao L, Xue Y Y, Chen F, Xiong Q, Meng R L, Ramirez D, Chu C W, Eggert J H and Mao H K 1994 *Phys. Rev. B* **50** 4260
[23] Einaga M, Sakata M, Ishikawa T, Shimizu K, Eremets M I, Drozdov A P, Troyan I A, Hirao N and Ohishi Y 2016 *Nat. Phys.* **12** 835
[24] Huang X L, Wang X, Duan D F, Bertil S, Li X, Huang Y P, Li F F, Zhou Q, Liu B, B and Cui T 2016 arXiv:1610.02630
[25] Zhang S J, Wang X C, Liu Q Q, Lv Y X, Yu X H, Lin Z J, Zhao Y S, Wang L, Ding Y, Mao H K and Jin C Q 2009 *Europhys. Lett.* **88** 47008
[26] Liu Q, Yu X, Wang X, Deng Z, Lv Y, Zhu J, Yang W, Wang L, Mao H, Shen G, Lu, Z, Ren Y, Chen Z, Lin Z, Zhao Y and Jin C 2011 *J. Am. Chem. Soc.* **133** 7892
[27] Birch F 1947 *Phys. Rev.* **71** 809
[28] Wang S, Yu X, Lin Z, Zhang R, He D Qin J, Zhu J, Han J, Wang L, Mao H, Zhang J and Zhao Y 2012 *Chem. Mater.* **24** 3023
[29] Ma T, Li H, Zheng X, Wang S, Wang X, Zhao H, Han S, Liu J, Zhang R, Zhu P, Long Y, Cheng J, Ma Y, Zhao Y, Jin C and Yu H 2017 *Advanced Mater.* **29** 1604003
[30] He D W, Shieh S R and Duffy T S 2004 *Phys. Rev. B* **70** 184121